Spectrochimica Acta Part B 66 (2011) 129–137

Contents lists available at ScienceDirect

Spectrochimica Acta Part B

journal homepage: www.elsevier.com/locate/sab

Integrated analytical methodologies for the study of corrosion processes in archaeological bronzes

Maria Francesca Alberghina, Rosita Barraco, Maria Brai, Tiziano Schillaci *, Luigi Tranchina

Dipartimento di Fisica e Tecnologie Relative, Laboratorio di Tecniche Fisiche per studio e caratterizzazione dei beni culturali (UniNetLab), Università di Palermo, Viale delle Scienze Ed. 18, 90128, Palermo, Italy

ARTICLE INFO

Article history:
Received 21 May 2010
Accepted 20 December 2010
Available online 28 December 2010

Keywords:
Corrosion patina
Bronze alloy
Integrated spectroscopy technique
Laser-induced breakdown spectroscopy (LIBS)
Archaeometry

ABSTRACT

The investigations on structure and micro-chemical composition of archaeological metal alloys are needed in archaeometry. The aim of this study is devoted both to acquire information about their provenance and production technology, and to improve our understanding about the corrosion processes. In this paper we present the study of the corrosion phenomena of bronze samples, laboratory-made according to binary, ternary and quaternary alloys typical of Roman archaeometallurgical production through an integrated methodology based on the use of non or micro invasive physical techniques. Among the analysed samples, two were artificially aged through burial in the archaeological site of Tharros, along the west coast of Sardinia (Italy). The corrosion products, typical of the bronzes in archaeological sites near the sea, have been characterized by non invasive and micro-destructive measurements. In particular, the corrosion patinas were examined through optical microscopy, scanning electron microscopy and microanalysis, X-ray fluorescence and laser ablation spectroscopy. The use of integrated technologies allowed us to determine both the elemental composition and surface morphology of the patina, highlighting the correlation between patina nature and chemical composition of the burial context. Moreover, data obtained by the laser-induced breakdown spectroscopy along the depth profile on the samples, have yielded information about the stratigraphic layers of corrosion products and their growth. Finally, the depth profiles allowed us to verify both the chemical elements constituting the patina, the metal ions constituting the alloy and the occurrence of migration phenomena from bulk to the surface.

1. Introduction

The study of the chemical degradation phenomena of the ancient metallic objects is a very complex task. These processes depend not only on many factors, such as: the chemical composition, the production techniques, but also on the environment and the type of soil in which the metal artefacts have been buried. The corrosion of metallic materials is a redox process that causes the deterioration and degradation of the physical–chemical properties of the material. In particular, the archaeological bronze artefacts present a corrosion patina that generally appears as a brownish-green or greenish-blue patina, especially when they are kept in corrosive environments. Various investigations have shown that the main constituents of the surface layer of the patina are green-coloured copper (II) compounds covering a red cuprous oxide layer in contact with the metal core of the alloy [1–4]. The environmental factors affect the formation of the copper (II) salts, in fact they could be malachite $Cu_2(CO_3)(OH)_2$ formed in soil, brochantite $CuSO_4 \cdot 3Cu(OH)_3$ in the atmosphere and atacamite $CuCl_2 \cdot 3Cu(OH)_2$ in the seawater. Mechanism of corrosion of bronze was often connected to copper chemistry, although lately it is increasingly emphasized in the role of alloying, which can significantly affect the corrosion behaviour of bronze [2–4].

The presence of lead plays a crucial role in the corrosion mechanism because during the solidification process of the alloy it tends to form intergranular *insulae* that become the place where the processes of corrosion are baited [1,5,6]. On the other hand, tin improves the resistance of the alloy to the growth of the corrosion patinas. In corrosion patinas, lead reach values up to four times higher than the content in the bulk [3]. Tin enrichment instead, due to the solubility and high stability of tin species, is strictly connected to the decuprification process [7]. The migration processes of the elements or ions along the analysed thickness of the alloy create a concentration gradient through the corrosion layer. Hence, the corrosion phenomena in archaeological bronzes can be understood with a multidisciplinary approach to characterize the chemistry and metallurgy of the corrosion patinas. Many analytical methods can be used to characterize the bronze corrosion product compositions. Moreover, the multi-analytical investigation can be useful to find a possible correlation between causes and effects aimed to highlight the

* Corresponding author. Tel.: +39 091 23899149; fax: +39 091 6615069.
E-mail address: tschillaci@unipa.it (T. Schillaci).

0584-8547/$ – see front matter.
doi:10.1016/j.sab.2010.12.010

occurring processes. The nature of corrosion patina (inhomogeneous and not uniformly distributed on metallic surface) and preservation of the integrity of the archaeological samples, require non or micro-destructive analytical methods [3,8–10].

Many of the used analytical techniques are able to yield also the stratigraphic data but they need a hand-made cross-section and sophisticated, expensive, and complex sampling that compromises the integrity of the sample [11]. In this context, the laser-induced breakdown spectroscopy (LIBS), in the past ten years has been extensively tested as an advanced tool for the characterization of objects of cultural interest and especially the metal ones [11]. It can provide depth-profiling information by successive laser pulses on the same point and sequentially acquired with a minimal damage [9,12–16].

The used techniques were X-ray fluorescence (XRF), optical microscopy (OM), electron microscopy with microanalysis (SEM-EDX) and laser induced breakdown spectroscopy (LIBS).

The comparison between XRF and LIBS techniques, here used, is particularly useful in the study of cultural heritage since their results are complementary in terms of both thickness and composition of the investigated surfaces [17,18]. According to this integrated investigative approach, bronze samples, that simulate the ancient Roman alloys [5,6,19,20] and whose corrosion has been induced by burial in the Roman archaeological site of Tharros along the west coast of Sardinia (Italy) [5], were analysed. In particular, the aim of this work is to follow (from the bulk up to surface) the chemical degradation evolution, analysing and characterizing the macroscopically distinguishable brownish or greenish patinas. Moreover, the contribution of the alloying elements to the growth of corrosion layers has been evaluated.

2. Experimental

Seven laboratory-made bronze samples of binary, ternary and quaternary alloys that reproduce the typical Roman metallurgical production were analysed. Chemical composition of samples, expressed as weight percentage, is reported in Table 1. Sulfur is also present as a consequence of the melting process. THT 128 and THT 129 samples have the same composition of CNR 128 and CNR 129, and were aged for one year by burial in the archaeological site of Tharros. The measurements were performed on each side of the samples, respectively A and B. XRF and LIBS spectrometers have been calibrated by analysing the bronze samples not affected by corrosion (CNR 8, CNR 9, CNR 20, CNR 128, and CNR 129) used as reference materials.

Measurements on THT 128 and THT 129 samples allowed us to study the corrosion products typical of bronzes in a site near the sea. In order to study the genesis and evolution of the corrosion patina, we chose to analyse both the typology of the patina: brownish and greenish patinas, so measurements were performed on many areas along the sample surface. Patinas were examined with the OM, XRF and LIBS spectrometers, SEM-EDX instrument. The integrated approach has provided information useful for the interpretation of the compositional and morphological data related to patina surfaces. The OM images (magnification 30×) were acquired by an OPTECH microscope equipped with a digital camera. With the aim to study both the surface morphology and the elemental composition, the corroded samples were examined by SEM and analysed by micro-analysis X-ray system (EDS). The experimental set-up values used for SEM-EDX measurements were: 20 kV(voltage), 240 μA (current), and 4.97×10^{-1} mbar (vacuum). XRF analyses were performed by using a portable X-ray fluorescence (XRF) instrument ArtTAX 200 (Bruker AXS). The ArtTAX is equipped with a low-power X-ray tube that is enclosed by a radiation shield, that guarantees the maximum safety when high voltage is on. An anode of molybdenum is used as a target. A filter disk system, put before the X-ray beam, was used in order to attenuate the Bremsstrahlung radiation and to reduce the diffracted component of X-ray beam. A pinhole system, in the X-ray source, provides collimated beam in the sample making available the instrument to perform spatially resolved multi-elemental analysis on three-dimensional structures. The X-ray fluorescence is detected by a XFlash detector (silicon drift detector) with high speed and low noise electronics with an energy resolution <145 eV at 5.9 keV. ArtTAX is equipped with a helium flux system for detection of light elements, since helium flux reduces the photoelectric absorption of characteristic X-rays emitted by the sample due to air molecules. For statistical reasons, five measures were acquired for each analysed point. It is important to note that, since the lead content is not uniformly distributed in bronze samples, its measurement varies significantly depending on the area selected for analysis. This shortcoming is avoided by averaging the measurements on different areas in the sample. The experimental set-up values used for XRF measurements were: for the molybdenum anode voltage and current, of 40 kV and of 600 μA respectively; an acquisition time of 300 s, and a helium flow rate of 1.6 l/min. The set-up parameters were selected in order to have a good spectral signal and to optimize the Signal to Noise Ratio (SNR). LIBS measurements were performed on the samples located inside a closed experimental chamber, equipped with a motorized table for exact positioning of the sample at the focus of the laser beams. LIBS instrument integrates a dual-pulse laser. Laser beam emits two collinear laser pulses at 1064 nm with an energy of 50–120 mJ per pulse with a maximum repetition rate of 10 Hz and a reciprocal delay adjustable from 0 to 60 μs. LIBS signal, either produced inside the experimental chamber or directly on the object, is collected through an optical fiber and sent to a compact Echelle spectrometer coupled to an intensified CCD camera for spectral acquisition. The instrument is controlled via an integrated personal computer which manages sample visualization and positioning, the experimental settings of the laser (energy of the beams, delay between the pulses, and repetition rate) and spectral acquisition parameters (number of spectra averaged, acquisition delay, CCD measurement gate and gain). Spectral resolution of the spectrometer is $\lambda/\Delta\lambda<5000$. LIBS spectra, after acquisition and storage, can be qualitatively and quantitatively analysed using proprietary software (LIBS++) which implements the calibration free-method, that it is useful to overcome the problem of the matrix effect [21]. In this work the calibration free-method was not used. Measurements of the peak intensity, for each spectral line characterizing the elements in the LIBS spectra, were performed. With the aim to characterize the profile distribution of the elements in the corroded samples, fifteen consecutive acquisitions were carried out on the brownish and on the greenish patinas in each side of the sample. Spectrum related to first shot was not included in the data-set, since it was not reproducible. The experimental set-up values used for the laser source and for the Echelle spectrometer were chosen with the aim to enhance the SNR. The instrumental set-up values were settled, for the laser source as the following: lamp laser energy of 16.5 J corresponding to an output laser energy of 60–70 mJ, repetition rate of 1 Hz, delay of the first laser pulse of 135 ms and the delay of the second laser pulse of 1 μs. For the CCD camera the set-up values were: number of accumulations of 5 spectra. The gain of multi channel plate

Table 1
Nominal composition of the bronze samples.

Sample label	Cu (%)	Sn (%)	Pb (%)	Zn (%)	S
CNR 8	95.0	5.0	–	–	–
CNR 9	85.0	15.0	–	–	–
CNR 20	97.0	3.0	–	–	–
CNR 128	92.3	7.5	0.2	–	Inclusions
CNR 129	82.3	3.0	0.5	14	Inclusions
THT 128	92.3	7.5	0.2	–	Inclusions
THT 129	82.3	3.0	0.5	14.0	Inclusions

was 230 and the gate pulse width and gate pulse delay were respectively 1.5 μs and 2.5 μs. The copper depth profile with a higher spatial resolution has been obtained by setting the CCD number of spectra accumulated to 2, the lamp laser energy to 12.5 J that corresponds to a value of 20–30 mJ and the gate pulse delay to 5 μs. A standard statistical analysis based on Principal Component Analysis (PCA) was performed to describe the obtained XRF results. The XLSTAT™ V. 5.7.0 software was used to perform PCA on data in order to reveal chemical differences among uncorroded bronze samples, greenish and brownish patinas. The analysis was conducted as parametric test using the Pearson similarity coefficient and generating two orthogonal vectors for principal components [22].

3. Results and discussion

Results, concerning structural and morphological characterization of patinas, are reported in terms of OM images, XRF spectra, and SEM-EDX data. Fig. 1 shows the OM images relative to the corroded samples, as example of microstructures characterized from a predominantly brown and/or green feature.

Fig. 2 shows the XRF spectra of the uncorroded samples (CNR 128 and CNR 129) and the brownish and greenish patinas of the corresponding corroded samples (THT 128 and THT 129). XRF spectra of the uncorroded samples show the presence of elements such as calcium and iron, and their presence is a consequence of the sample preparation. The corrosion process modifies the chemical composition of the sample by introducing elements coming from the burial environment such as silicon, chlorine and manganese as shown by the XRF spectra. Moreover, an increase of spectral line intensities corresponding to calcium and iron elements is also observed.

SEM images with different magnifications of two different areas of the corroded samples are reported in Fig. 3, elemental composition, measured by the EDX microanalysis, is also shown. Samples show the same elemental composition, but differences among percentage of the elements confirm an evident inhomogeneity in the morphological and structural aspects of the corrosion products in both corroded samples. The similarity/dissimilarity among samples on the basis of their chemical composition on XRF data was performed by a PCA. Results are reported in Fig. 4 by a bi-plot of the samples in the subspace spanned by the first two principal components F_1 and F_2 accounting for 58.10% and 31.23% of the total variability, respectively.

The points enclosed in the dashed line correspond to 128 samples (CNR and THT 128), those in the dash-dotted line to the 129 samples (CNR and THT 129). Squares indicate the uncorroded samples, the full and empty triangles the greenish patina sides A and B, respectively. Same criterion is valid for the full and empty circles related to the brownish patina.

PCA data make possible to distinguish the typology of the sample (128 and 129) and also the colour of the patina i.e. brown or green. Moreover, for what concerns the green patina, the PCA allows to select the measurement points for each side (A and B). In particular, THT 128 sample exhibits evident differences in the tin content, whereas THT 129 sample in the lead content one. Furthermore, it is not possible to distinguish brownish patina of side A from B that is instead collected only in one cluster for each sample. Thus, PCA permits to display the contribution of each element participant to the growth of the corrosion layer confirming the succession (original alloy, brownish and greenish patinas) of the patina formation in the degradation process. In fact, results obtained by measurement on brownish patina are plotted in the PCA, closer to that corresponding at the original

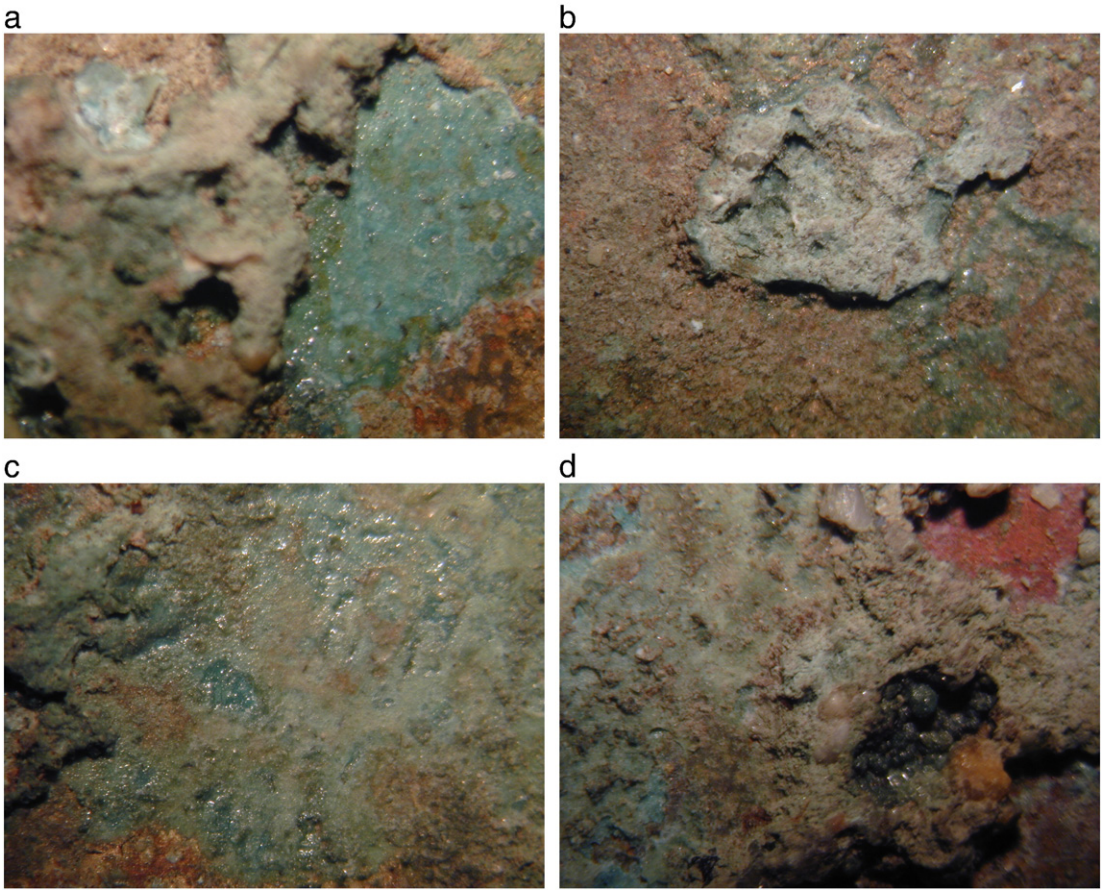

Fig. 1. OM images of typical surface corrosion of greenish and brownish patinas on (a, b) THT 128 and (c, d) THT 129 samples, respectively.

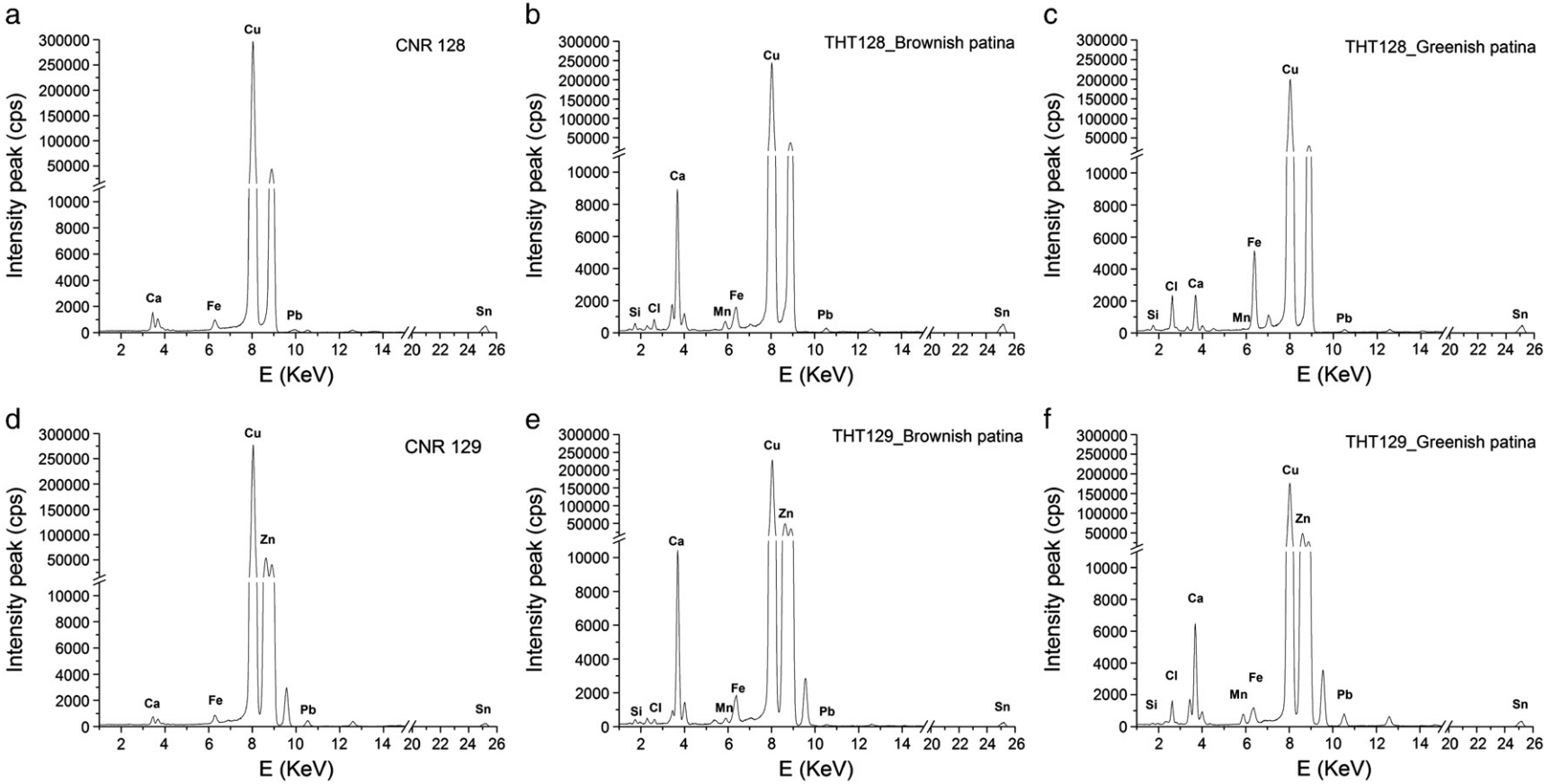

Fig. 2. Typical XRF spectra of the uncorroded sample CNR 128 (a), brownish and greenish patinas on THT 128 (c, d); and analogues spectra of CNR 129 (d) and THT 129 (e, f).

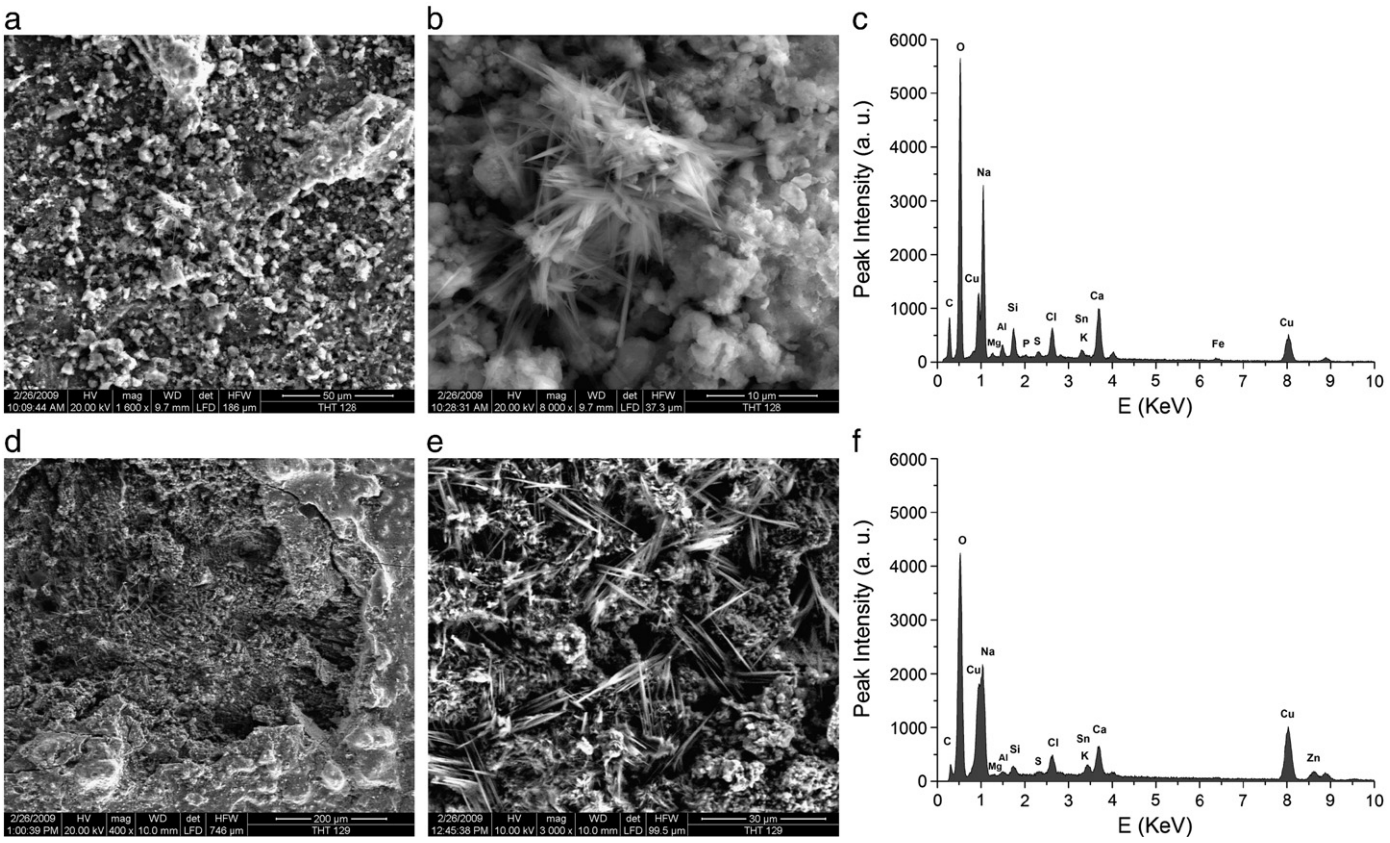

Fig. 3. SEM images with different magnifications and relative EDX spectra of typical surface corrosion of the patinas on THT 128 (a, b, c) and THT 129 (d, e, f), respectively.

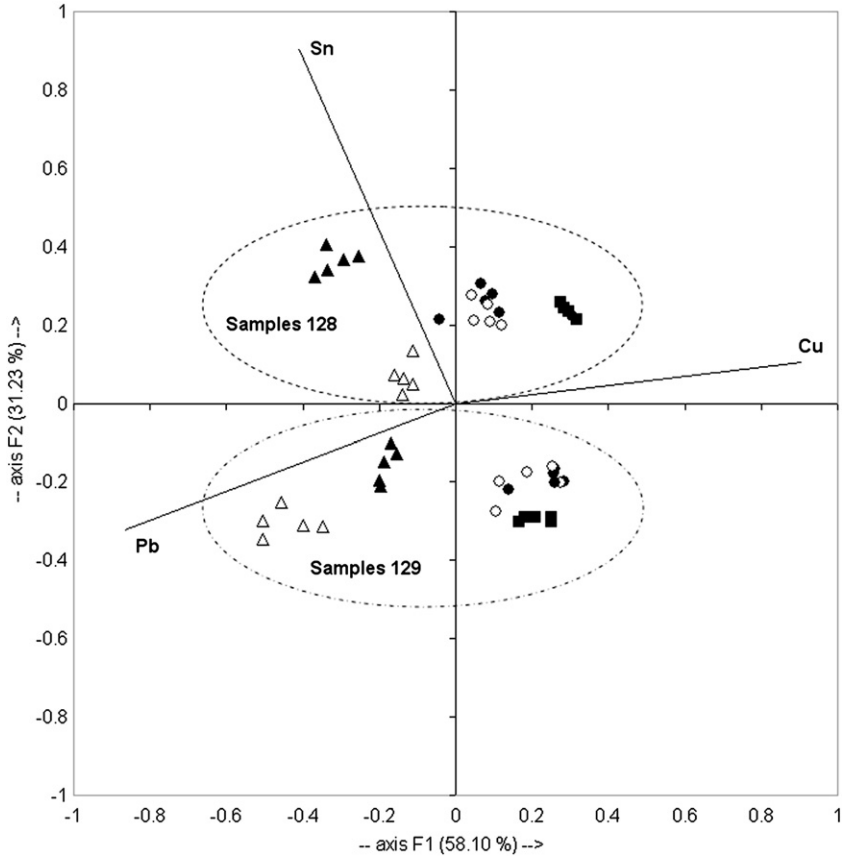

Fig. 4. Bi-plot of the samples in the subspace spanned by the first two principal components F_1 and F_2.

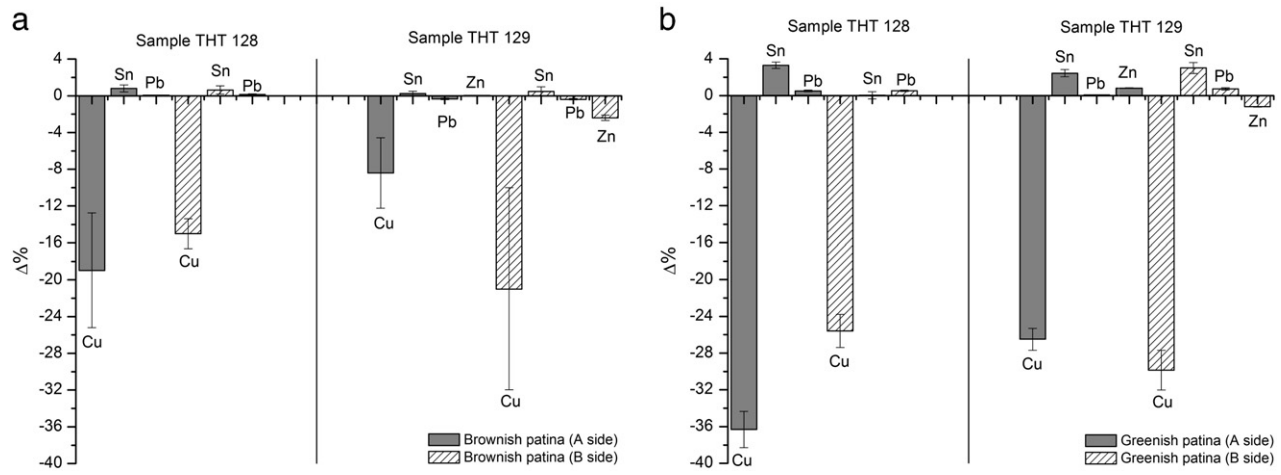

Fig. 5. Bar plot of the variation expressed as percentage, of each element present in the patinas of the degraded samples with respect to the uncorroded samples. Panels (a) and (b) are related to the brownish and greenish patinas, respectively.

composition of the alloy than the greenish ones. This behaviour could be also due to the presence of the Zn, whose contribution is not considered in the PCA, but instead involves in the alloy formation and, hence in alloy properties.

Fig. 5 reported a bar plot, the variation of which is expressed as percentage of each element present in the patinas of the degraded samples (THT 128 and THT 129) with respect to the uncorroded ones (CNR 128 and CNR 129). Panels (a) and (b) are related to the brownish and greenish patinas, respectively. Error bars represent the standard deviation associated to the concentration difference expressed in percentage, between the uncorroded and the degraded samples. The variability of the width of the error bars depends on the inhomogeneity of the corrosion layers in terms of thickness and composition.

Cu content reduction, as expected, is the more evident effect of the corrosion process characterizing both the patinas. Nevertheless, the largest variations occur in the greenish patinas. These considerations are in good agreement with the Sn enrichment [7] in the corrosion layer. Sn enrichment factor, denoted with $f(\mathrm{Sn})$, can be calculated according to Eq. (1):

$$f(\mathrm{Sn}) = \left[\frac{\mathrm{Sn}/(\mathrm{Sn}+\mathrm{Cu})_{patina}}{\mathrm{Sn}/(\mathrm{Sn}+\mathrm{Cu})_{uncorroded\ sample}}\right] \quad (1)$$

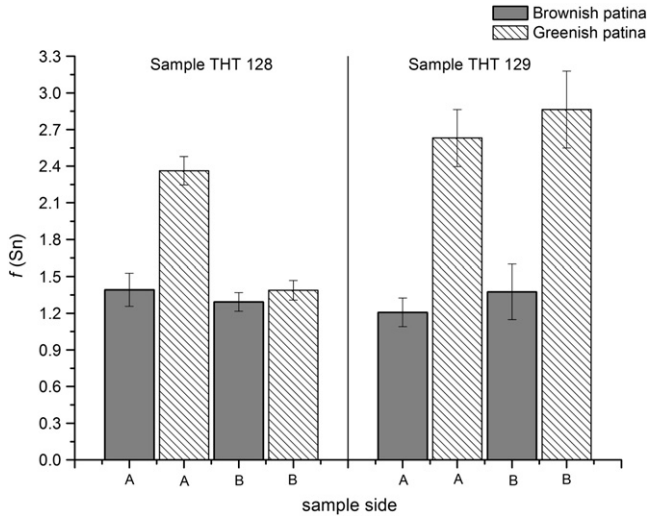

Fig. 6. Bar plot of the Sn enrichment of the corroded sample (brownish and greenish patinas) with respect to the corresponding uncorroded sample.

where Sn and Cu are the XRF peak intensity area measured both on the greenish and brownish patinas of the degraded (THT 128 and THT 129) and on the uncorroded samples (CNR 128 and CNR 129). Increasing of tin and reducing of copper contents in the corrosion layers can be explained by the copper selective dissolution causing its removal from the alloy (decuprification process) as proposed by Robbiola et al. [2]. Fig. 6 shows the bar plot of $f(\mathrm{Sn})$ in the brownish and greenish patinas for each side of the corroded sample (THT 128 and THT 129). It can be noticed that, the brownish patinas present a comparable increasing of tin content in whole set of samples, despite that they belong to two different typologies of alloys (quaternary and ternary). The greenish patinas show a greater tin enrichment than the brownish ones. Moreover, the greenish patina of the samples containing Zn (THT 129) presents a larger Sn enrichment than the greenish patina of the samples of ternary alloy (without Zn). Tin content, for the brownish patina, keeps almost constant for whole set of the measurements, on the contrary it is affected by fluctuations in the greenish ones. This finding can be explained by considering the larger stability of brownish than greenish patina.

In order to describe the behaviour of elements in the alloy, beyond the investigable thickness by XRF (about 60–70 μm with our instrumental set-up), LIBS depth profiles were carried out by subsequent ablation of the sample surface at the same irradiated spot. In this way, it was possible to integrate the superficial data detected by XRF technique with those acquired by LIBS. The spectral lines selected for the study of the depth profiles (plots of signal

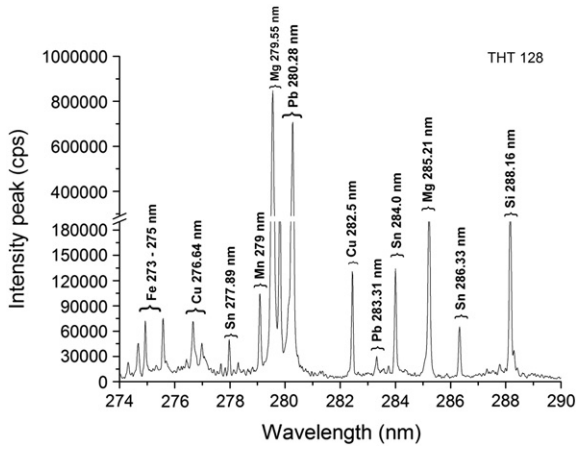

Fig. 7. Typical LIBS spectrum of the corroded sample THT 128.

intensity versus shot numbers) were 280.2 nm for Pb (I), 282.5 nm for Cu (I), and 286.3 (I) for the Sn. Fig. 7 shows a typical LIBS spectrum for the THT 128 sample. Copper also chose the spectral line 521.8 nm (Cu I) due to the high intensity probability.

Fig. 8 represents the depth profiles of the intensity ratios of each set of five accumulated laser shots with respect to the tenth laser shots accumulation for lead, tin and copper respectively, measured on the uncorroded samples (CNR 128 and CNR 129) and on the greenish and

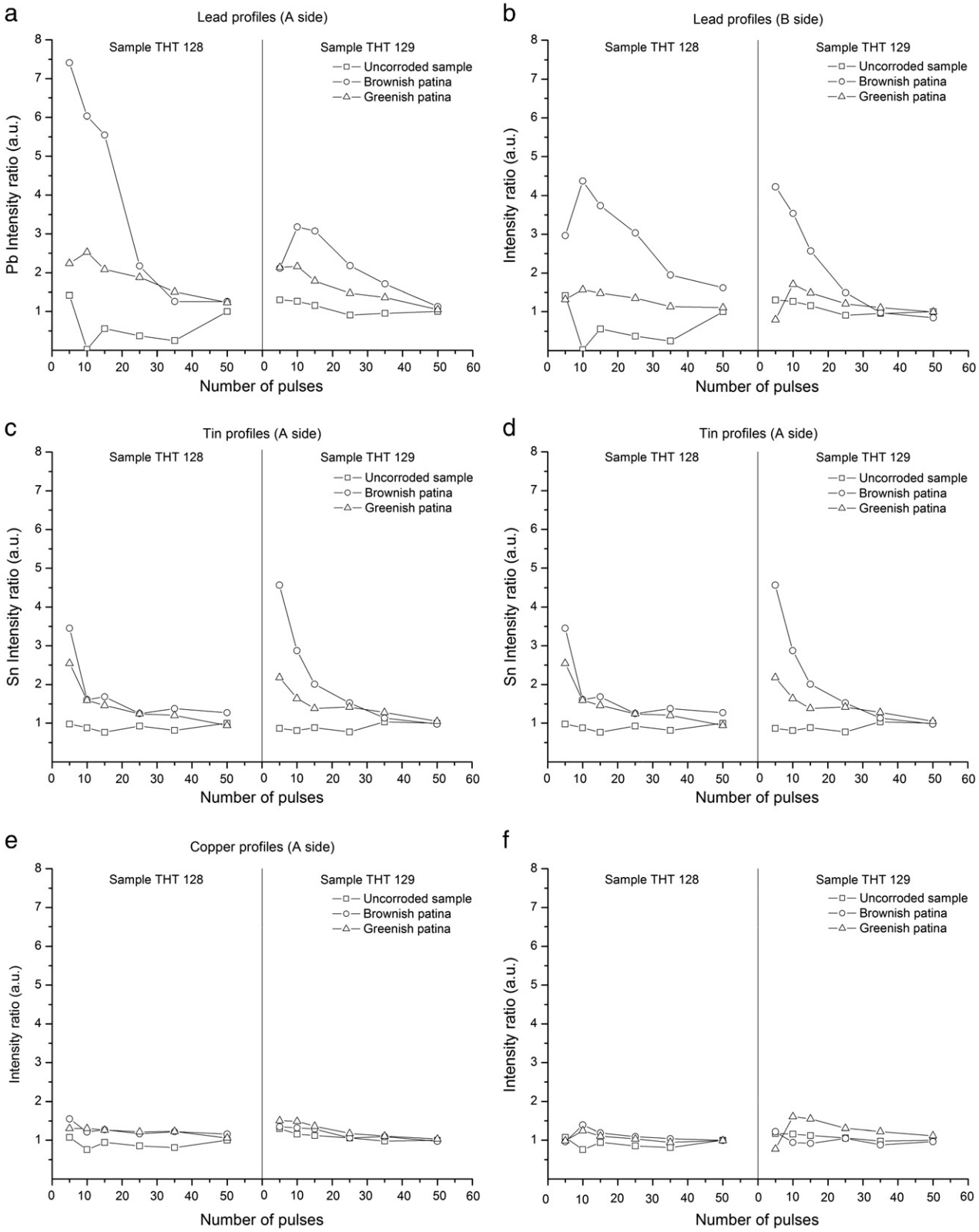

Fig. 8. Depth profiles of (a, b) lead, (c, d) tin and (e, f) copper for the uncorroded samples (CNR 128 and CNR 129) and the brownish and greenish patinas of corroded samples (THT 128 and THT 129) with respect to each element side (A and B).

brownish areas of the degraded samples (THT 128 and THT 129). The choice of plotting these ratios derives from the attempt to avoid the eventual differences in the metal properties that do not guarantee the same stoichiometry ratios of the plasma with respect to the original evaporated surface [12,15,21]. Moreover, this decision is justified by our interest to evaluate the relative variations of the elements along the different structural layers of the bronze artefact (i.e. greenish, brownish patinas and metal alloy). The depth profiles, shown in Fig. 8, allowed us to evaluate the contribution of the alloy elements to the growth of the corrosion layers, by following their distribution along the analysed thickness up to bulk. The intercomparison between the uncorroded and the corroded sample guarantees to achieve this condition.

The behaviour of the lead profiles varies widely from point to point due to the low lead concentration and to the inhomogeneous distribution of this element in the alloy. However, regarding the investigated points, LIBS measurements confirmed the migration phenomenon of lead from bulk to surface [2,3], as already discussed (see the PCA on XRF data related to the outer layers reported in Fig. 4). It not was possible to achieve LIBS measurements for smaller thickness (<100 μm) because of the difficulties in detecting lead by using the chosen instrumental set-up. In fact, the parameters were selected in order to obtain a statistically stable peak intensity for the minor constituent as lead and tin respectively and that present a different stoichiometry time resident in the plasma [15]. The tin profiles show a different behaviour for both, side and samples, even if in every case a tin enrichment has been observed. These findings agree with the results previously showed (see Figs. 5 and 6), and confirm that an enrichment of tin affects a deep thicknesses that cannot be investigated by XRF measurements. According to the previous results, the relative tin enrichment can be explained by the low solubility and high stability of tin species, allowing the tin ions to remain in the patina [2]. Nevertheless, also in this case, it was not possible to realize LIBS measurements related to thickness <100 μm because of the difficulties described in the case of lead. The behaviour of the copper profiles of the two degraded samples (THT 128 and THT 129), remains approximately constant. However, even for these investigated thicknesses, just in some cases, it was possible to observe that the low values of the intensity ratios reveal the lower Cu content in the surface than in the bulk, confirming the decuprification process already verified by XRF investigations (see Figs. 4 and 5). Differently from lead and tin, it was possible, for copper, to achieve LIBS measurements for smaller thickness (<100 μm) by using a new set of instrumental parameters keeping a good detection efficiency. The LIBS data, in fact, have provided complementary information about the different behaviours of the alloy elements. Nevertheless, they are not directly comparable with XRF data shown in Fig. 5 since they refer to different investigated thicknesses. To overcome this problem, a new set of data have been acquired with suitable LIBS parameters which have allowed to analyse depth profiles with higher spatial resolution. In this way, it was possible to investigate the outer layers of thickness comparable with those analysed by XRF and negligible by the previous LIBS results. Fig. 9 shows the copper depth profiles for the greenish patina for the degraded samples. Data are related to the spectral line 521.8 nm (Cu I), for greenish patina in 128 (empty triangles) and 129 samples (grey triangles), and were normalised to the mean values of the peak intensity of the corresponding not degraded sample. As shown in Fig. 9, data were well fitted by a lognormal function that is characterized by the fact that it introduces a point of maximum analytically determined. In order to achieve a linear signal level, for THT 128 and THT 129 samples 8 and 14 laser shots respectively, were necessary. This finding allowed us to discriminate the corrosion layers with different thicknesses. Particularly, through the corroded layer thickness up to bulk, copper shows an increment in concentrations and these results are in agreement with those obtained by XRF analysis.

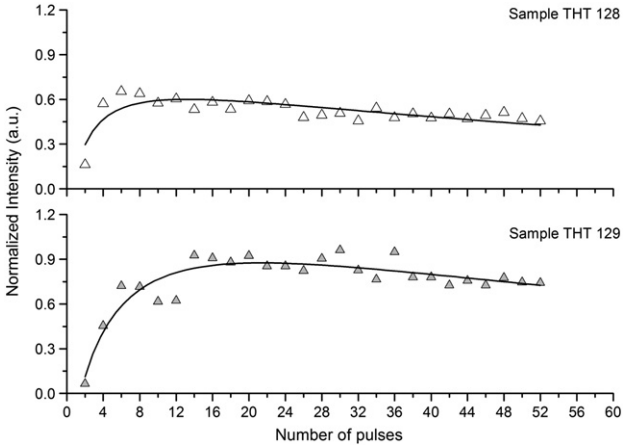

Fig. 9. Copper depth profiles of the degraded samples (THT 128 and THT 129) relative to the greenish patina.

Moreover, reaching the bulk by repeated laser pulses, copper concentrations show a decreasing trend. This findings need further study to investigate the phenomena occurring in the deeper part of corrosion layer where bulk and corrosion layers are strictly combined. In order to convert laser shot numbers into depth values, SEM images (acquired with different tilt angles) of the corroded samples, were employed. An averaged ablation rate value of about 15 μm per pulse was estimated. The results corroborate that the investigated thickness of the corrosion layers may change between 100 and 250 μm above the bronze matrix.

4. Conclusions

The present study confirms the versatility and the analytical ability of non-invasive or micro-destructive physical techniques in providing a clear response to the investigation needs in the study of complex archaeological samples. An appropriate investigative methodology allowed us, in fact, to characterize the altered surfaces of bronze samples and to determine the chemical composition of the corrosion layers and its variation along analysed thickness. Analyses permitted the characterization of typical corrosion features present on bronze objects, allowing to evaluate one of the factors which mainly influence the growth of the corrosion layers, i.e. the alloying elements. Moreover, significant information on the behaviour of the elements constituting the alloy and, their migration from the bulk to the corrosion layer has been obtained. In particular, for what concern the distribution of the alloy elements in the patina, two kinds of behaviour are evidenced by the LIBS measurements. Depth profiles make possible to distinguish different typologies of the behaviour in the samples. Particularly, in the deeper part of corrosion layers, lead shows a great trend variability due to the different natures of the analysed areas (greenish or brownish), tin concentrations seem to increase through the thickness of the patina and, on the contrary, copper concentrations assume an almost constant value. A new set of LIBS parameters chosen in order to obtain a higher spatial resolution, allowed us to study the behaviour of copper through the whole corroded layer thickness up to bulk. Particularly, copper shows a concentration increment through the corroded layer thickness up to bulk, these results are in agreement with those obtained by XRF analysis. After reaching the bulk by repeated laser pulses, copper concentrations show a decreasing trend. These findings need further study to investigate the phenomena occurring in the deeper part of corrosion layer where bulk and corrosion layers are strictly combined. Integrated investigation has been able to provide information about the distribution of elements constituting the alloy along the corroded thickness. LIBS technique allowed us “to discretize” the investigated

volume in order to compare similar thickness with respect to the XRF data, so it is possible to integrate the XRF findings thanks to the ability of LIBS technique to discriminate the information about the composition along the thickness of the investigated layer. In order to perform a more accurate quantitative LIBS analysis, further works will be devoted to the evaluation of the ablated mass for each laser shot for different chemical and physical properties of materials. Moreover, the research should be directed to understand how the LIBS parameters (laser energy and CCD parameters) can affect the plasma composition and its time evolution in order to follow also the behaviour of tin and lead through the corrosion layers.

Acknowledgements

The authors would like to thank Mr. Marcello Mirabello for the technical support. This research has been conducted within the project PRIN 2007 “Optimization of integrated physical techniques of X-ray spectrometry, laser and electron spin for the study of corrosion processes on surface and volume of metals and alloys”, funded by the Italian Ministry for University and Scientific Research.

References

[1] G.M. Ingo, T. De Caro, C. Riccucci, E. Angelini, S. Grassini, S. Balbi, P. Bernardini, D. Salvi, L. Bousselmi, A. Cilingiroglu, M. Gener, V.K. Gouda, O. Al Jarrah, S. Khosroff, Z. Mahdjoub, Z. Al Saad, W. El-Saddik, P. Vassiliou, Large scale investigation of chemical composition, structure and corrosion mechanism of bronze archaeological artefacts from Mediterranean basin, Appl. Phys. A 83 (2006) 513–520.
[2] L. Robbiola, J.M. Blengino, C. Fiaud, Morphology and mechanisms of formation of natural patinas on archaeological Cu–Sn alloys, Corros. Sci. 40 (1998) 2083–2111.
[3] E. Figueiredo, P. Valerio, M.F. Araujoa, J.C. Senna-Martinez, Micro-EDXRF surface analyses of a bronze spear head: lead content in metal and corrosion layers, Nucl. Instrum. Methods Phys. Res. A 580 (2007) 725–727.
[4] I. De Ryck, E. Van Biezen, K. Leyssens, A. Adriaens, P. Storme, F. Adams, Study of tin corrosion: the influence of alloying elements, J. Cult. Herit. 5 (2004) 189–195.
[5] G.M. Ingo, T. De Caro, C. Riccucci, S. Khosroff, Uncommon corrosion phenomena of archaeological bronze alloys, Appl. Phys. A 83 (2006) 581–588.
[6] I. Constantinides, M. Gritsch, A. Adriaens, H. Hutter, F. Adams, Microstructural characterisation of five simulated archaeological copper alloys using light microscopy, scanning electron microscopy, energy dispersive X-ray microanalysis and secondary ion mass spectrometry, Anal. Chim. Acta 440 (2001) 189–198.
[7] H. Hassairi, L. Bousselmi, E. Triki, G.M. Ingo, Assessment of the interphase behaviour of two bronze alloys in archaeological soil, Mater. Corros. 58 (2007) 121–128.
[8] J.A. Perez-Serradilla, A. Jurado-Lopez, M.D. Luque de Castro, Complementarity of XRFS and LIBS for corrosion studies, Talanta 71 (2007) 97–102.
[9] M. Ferretti, G. Cristoforetti, S. Legnaioli, V. Palleschi, A. Salvetti, E. Tognoni, E. Console, P. Palaia, In situ study of the Porticello bronzes by portable X-ray fluorescence and laser-induced breakdown spectroscopy, Spectrochim. Acta Part B 62 (2007) 1512–1518.
[10] L. Cartechini, R. Rinaldi, W. Kockelmann, S. Bonamore, D. Manconi, I. Borgia, P. Rocchi, B. Brunetti, A. Sgamellotti, Non-destructive characterization of compositional and textural properties of Etruscan bronzes: a multi-method approach, Appl. Phys. A 83 (2006) 631–636.
[11] F.J. Fortes, M. Cortés, M.D. Simòn, L.M. Cabalìn, J.J. Laserna, Chronocultural sorting of archaeological bronze objects using laser-induced breakdown spectrometry, Anal. Chim. Acta 554 (2005) 136–143.
[12] A. Elhassan, A. Giakoumaki, D. Anglos, G.M. Ingo, L. Robbiola, M.A. Harith, Nanosecond and femtosecond Laser Induced Breakdown Spectroscopic analysis of bronze alloys, Spectrochim. Acta Part B 63 (2008) 504–511.
[13] F.J. Fortes, L.M. Cabalín, J.J. Laserna, The potential of laser-induced breakdown spectrometry for real time monitoring the laser cleaning of archaeometallurgical objects, Spectrochim. Acta Part B 63 (2008) 1191–1197.
[14] A. De Giacomo, M. Dell'Aglio, F. Colao, R. Fantoni, V. Lazic, Double-pulse LIBS in bulk water and on submerged bronze samples, Appl. Surf. Sci. 247 (2005) 157–162.
[15] L. Fornarini, F. Colao, R. Fantoni, V. Lazic, V. Spizzichino, Calibration analysis of bronze samples by nanosecond laser induced breakdown spectroscopy: a theoretical and experimental approach, Spectrochim. Acta Part B 60 (2005) 1186–1201.
[16] A. Giakoumaki, K. Melessanaki, D. Anglos, Laser-induced breakdown spectroscopy (LIBS) in archaeological science—applications and prospects, Anal. Bioanal. Chem. 387 (2007) 749–760.
[17] M.F. Alberghina, R. Barraco, M. Brai, T. Schillaci, L. Tranchina, Double laser LIBS and micro-XRF spectroscopy applied to characterize materials coming from the Greek–Roman theater of Taormina, Proceedings of SPIE Europe optics metrology, Optics for Arts, Architecture and Archaeology II, Vol. 7391, 739107, Munich, Germany; 2009.
[18] M. Brai, T. Schillaci, L. Tranchina, Double laser LIBS applied to natural and artificial materials from cultural heritage. A comparison with micro-XRF analysis, Spectrochim. Acta Part B 64 (2009) 1119–1127.
[19] I. Constantinides, A. Adriaens, F. Adams, Surface characterization of artificial corrosion layers on copper alloy reference materials, Appl. Surf. Sci. 189 (2002) 90–101.
[20] C. Chiavari, A. Colledan, A. Frignani, G. Brunoro, Corrosion evaluation of traditional and new bronzes for artistic castings, Mater. Chem. Phys. 95 (2006) 252–259.
[21] E. Tognoni, G. Cristoforetti, S. Legnaioli, V. Palleschi, Calibration-free Laser-Induced Breakdown Spectroscopy: state of the art, Spectrochim. Acta Part B 65 (2010) 1–14.
[22] K. Pearson, Principal Components Analysis, The London, Edinburgh and Dublin Philosophical Magazine and Journal 6 (1901) 566.